CONF-900944--52

SSCL-405

SSCL-405

Superconducting Super Collider Laboratory

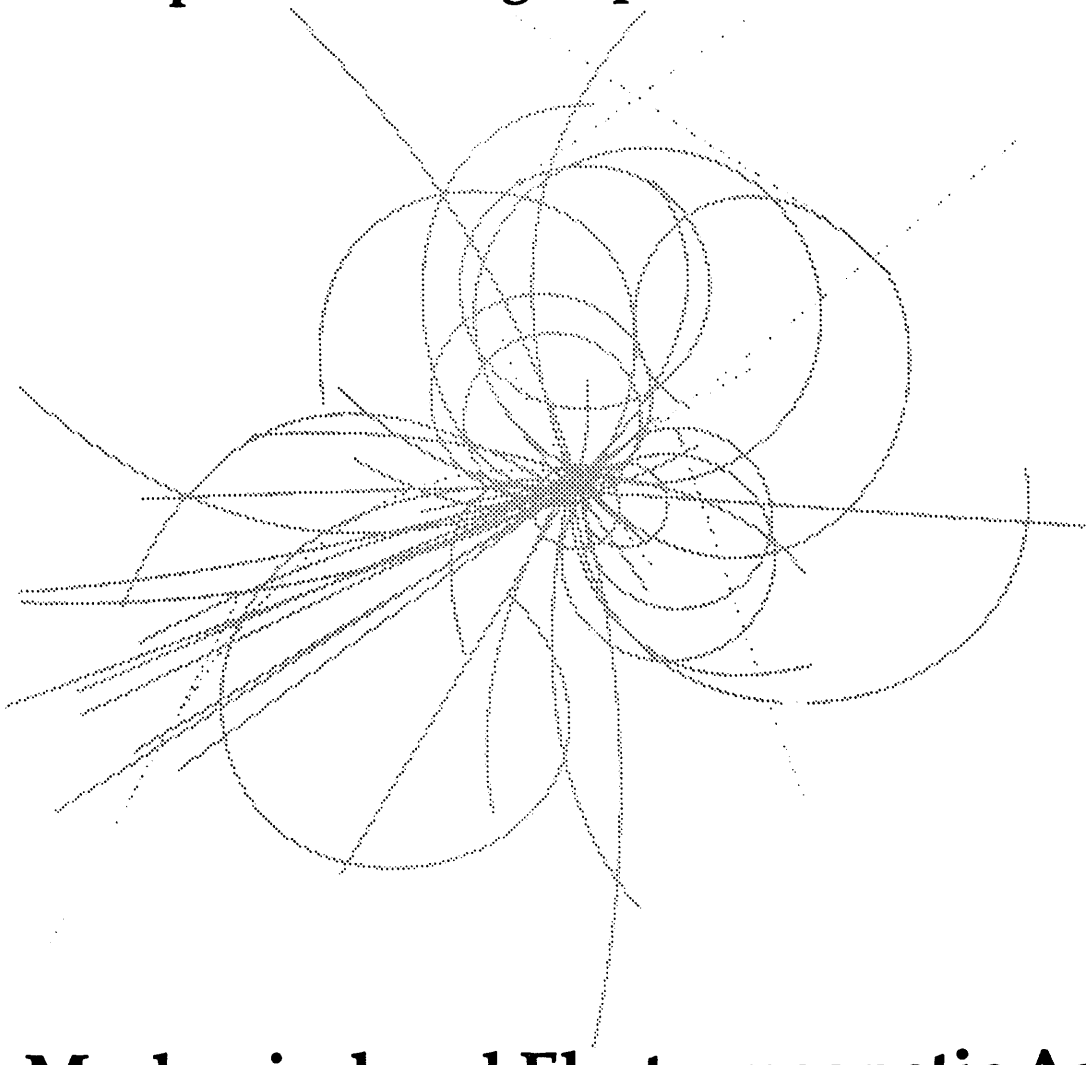

Mechanical and Electromagnetic Analysis of 50 millimeter Designs for the SSC Dipole

J. Jayakumar, K. Leung, F. Nobrega, D. Orrell, P. Sanger, G. Snitchler, G. Spigo, and J. Turner, et al

September 1990

OCT 2 2 1991

DISTRIBUTION OF THIS DOCUMENT IS UNLIMITED

SSCL--405

DE92 001659

Mechanical and Electromagnetic Analysis of 50 millimeter Designs for the SSC Dipole*

J. Jayakumar, K. Leung, F. Nobrega, D. Orrell, P. Sanger, G. Snitchler, G. Spigo, and J. Turner, et al

Magnet Division
Superconducting Super Collider Laboratory†
2550 Beckleymeade Ave.
Dallas, TX 75237

September 1990

*Submitted to the Applied Superconductivity Conference, Snowmass, Colorado, September 24–28, 1990.
†Operated by the Universities Research Association, Inc., for the U.S. Department of Energy under Contract No. DE-AC02-89ER40486.

MASTER

DISTRIBUTION OF THIS DOCUMENT IS UNLIMITED

MECHANICAL AND ELECTROMAGNETIC ANALYSIS OF 50 MILLIMETER DESIGNS FOR THE SSC DIPOLE.

J. Jayakumar, K. Leung, F. Nobrega, D. Orrell,
P. Sanger, G. Snitchler, G. Spigo, J. Turner
SSC Laboratory
2550 Beckleymeade Avenue - Dallas - TX - 75237

C. Goodzeit, R. Gupta, S. Kahn, G. Morgan, E. Willen
Brookhaven National Laboratory
Upton - Long Island - NY - 11973

J. Kerby, J. Strait
Fermi National Accelerator Laboratory
Pine & Kirk Roads - Batavia - IL - 60510

R. Schermer
Lawrence Berkeley Laboratory
One Cyclotron Road - Berkeley - CA - 94720

Abstract

Several designs for the Superconducting Super Collider dipole magnet have been analyzed. This note discusses the mechanical and electromagnetic features of each design. Electromagnetic and Mechanical analyses were performed using hand, computer programs and finite element techniques to evaluate the design.

Introduction

The Superconducting Super Collider requires about 8000 dipole magnets with an aperture of 50 mm and field intensity of 6.65 T. The salient parameters of the magnet are shown in Table 1. A concerted program of development and testing is in progress at BNL, FNAL and SSCL, to prove design concepts and prepare for industrialization. The following paper describes the design studies carried out on various aspects of the cold mass design for this particular magnet. Design studies on the 2D magnetic and structural aspects, coil ends and magnet ends are reported. Different design options, evaluated for magnet ends, are also reported.

Table 1. Main Parameters of the 50 mm dipole Cross-Section

Coil Inner Diameter	50.00 mm
Coil Outer Diameter	99.42 mm
Yoke Inner Diameter	135.62 mm
Yoke Outer Diameter	327.3 mm
Shell Outer Diameter	340 mm
Coil Straight Length	14880 mm
Overall Coil Length	15165 mm
Nominal Induction B_0	6.65 T
Ratio of Peak Field to B_0	1.048
Operation Current at B_0	6553 A
Resultant of EM Forces at B_0 ... Fx	963 N/mm
in the First Coil Quadrant ..... Fy	409 N/mm
Inner Layer	
Number of turns	19
Cable Geometry	1.326, 1.588 x 12.12 mm^2
Number of Strands	30
Wire Diameter	.808 mm
Cu/Sc Ratio	1.5
Outer Layer	
Number of turns	26
Cable Geometry	1.064, 1.270 x 11.68 mm^2
Number of Strands	36
Wire Diameter	.648 mm
Cu/Sc Ratio	1.8
NbTi Filament Diameter	6 μm

Magnetic Design of the Dipole

The baseline dipole cross-section DSX201, designed at BNL (1), is shown in Figure 1. It consists of 45 turns in two layers; the inner layer has 19 turns of 30 strand cable, the outer 26 turns of 36 strand cable. There are three wedges in the coil inner layer and one in the outer. The DSX201 gives good harmonics and field margin and is being used for test magnets. The cable dimensions have now been changed slightly necessitating a new design, being developed in SSCL.

The objective of the cross-section design is to provide the desired field harmonics and conductor margin while keeping superconductor volume and design complexity to a minimum. At the SSC, coil locations are optimized to give the desired harmonics using the code COP6. Fields are calculated analytically (the iron is considered to be circular and infinitely permeable). The configuration is optimized to give the best RMS fit to the desired harmonics, subject to certain constraints such as minimum wedge size.

With DSX201 the iron yoke contributes approximately 22% of the total field of 6.65 tesla. Saturation of the iron with increasing current affects the transfer function (the ratio of the central field to current),b2 and, to a smaller extent, higher harmonics. This has been studied using PE2D® (2) which is a commercially available finite element code. The b2 saturation can be controlled to some

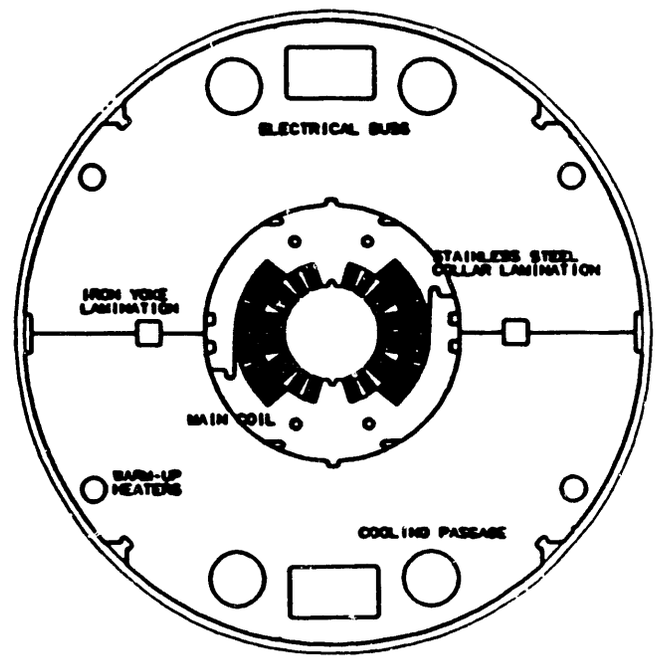

Figure 1. DSX201 Cold Mass Cross-Section

extent by careful sizing and location of the yoke alignment key. The variation of transfer function and harmonics with current is shown in Figure 2. The specifications on field harmonics dictated by beam aperture needs is shown with design values in Table 2. Harmonics are expressed as parts in 10^4 of the main field evaluated at a 1 cm radius from the magnet center. A contour plot of the magnetic potential is given in figure 3.

For obtaining the conductor margin, peak fields are calculated analytically and with PE2D®. For DSX201 the ratio of peak to central field is 1.048. Critical Surface Margin is usually expressed as a percentage amount above the specified field (or current). DSX201 has a calculated margin of 10% above 6.6 Tesla.

Table 2. Desired and Optimized values of low field harmonics in prime units of 10^{-4} for the DSX201 Cross-Section

Values	b_2'	b_4'	b_6'	b_8'	b_{10}'	b_{12}'
Desired	0	0	0±.05	±(.04to.05)	0±.05	0±.05
Optimized	0	0	-0.004	0.044	0.014	-0.001

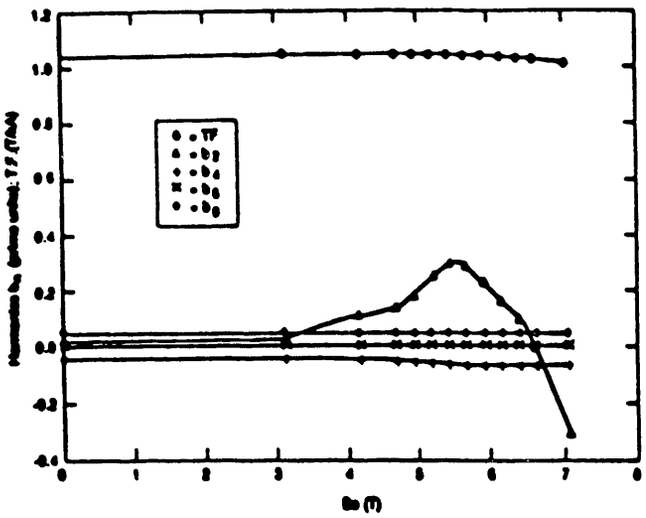

Figure 2. Variation of Transfer Function and Harmonics with Bo

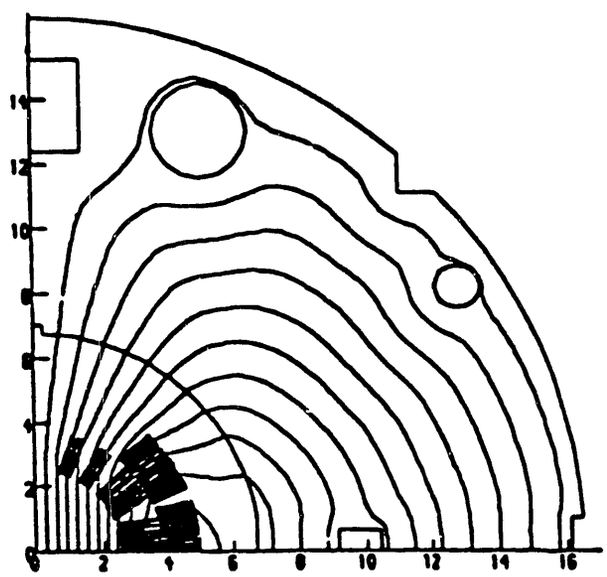

Figure 3. Contour Plot of the Magnet Potential in the DSX201 Cross Section

Mechanical Design of 2D Cross Section

In the framework of the mechanical studies for the SSC dipole, three possible geometries are envisaged.

Case 1: Stainless steel collars and horizontally split yoke (3).
Case 2: Stainless steel collars and vertically split yoke (4).
Case 3: Aluminium collars and vertically split yoke with an aluminium bar inserted in the yoke to control the gap (5).

Studies were carried out for these three geometries, in the context of optimizing and understanding the designs and are not intended for comparison.

Figure 1 shows the main dimensions of the cross section that is quite similar for all the solutions. The two coil layers have different superconducting cable, with thinner strands in the outer layer to have the adaptation (grading) of the current density to the maximum field seen by the winding. All the wedges are of copper. The coils are surrounded by laminated collars which are clamped together by keys at the midplane. The iron yoke is split in two symmetric parts which are mounted around the collars under a compressive force. They are clamped around the collars by a stainless steel cylinder, made from two welded halves.

The mechanical analysis has been performed by hand and with the finite element code ANSYS® (6). In these calculations creep characteristics of the coils were not taken into account and all the coils characteristics are assumed to be linear and follow Hooke's law. The magnetic forces were calculated in ANSYS® assuming a infinite permeability iron.

The main objective of the design is to have no region of coil under tension and to have the coils always in contact with the collars. To avoid or limit the creep effects in the coils (flow of the insulating materials) that mainly occur at room temperature it is very important to have the coil prestress as small as possible at room temperature. To estimate this value one may assume an infinitely rigid mechanical structure so that the radial Lorentz force on the coils may be ignored. Further, assuming zero friction, the azimuthal forces are balanced. Also, the stresses due to the bending moments in the coils are neglected. A first idea of the minimum prestress in the coils at room temperature at the pole location is given by:

$$\sigma_{pole} = \frac{2F_L^{\theta}}{3W} \pm \Delta\alpha * E$$

in which W is the width of the insulated cable, E Young's modulus of the coil, and $\Delta\alpha$ is the difference of the integrated thermal contraction coefficient between 4 and 300 K for coils and collars and F_L^{θ} is the integrated azimuthal Lorentz force in the coil.

The calculations have shown that, in some aspects, the different geometries have common behavior. For all the schemes the horizontal deflection after collaring is very small in absolute value and almost negligible compared to the vertical deflection. This can be explained by considering the collar as a ring in which a radial pressure and a force acting in vertical direction are applied. The deflection due to the bending moment acting at the midplane given by the vertical force counteracts the deflection due to the pressure.

Collaring

For the first geometry two different shapes of collars have been analyzed (round and anti-oval collars (the vertical axis is less than the horizontal)). The required prestress in the coil at room temperature is simulated with an azimuthal pressure of 70 and 56 MPa on the first and second layer respectively. For both the analyses the azimuthal pole stresses have almost the same values mentioned above. For the second geometry which uses another shape of collars (elliptical with a horizontal major axis) the prestress is simulated by the insertion of shims at the horizontal midplane. The values of the pole stress is comparable to the previous solution. For the third geometry the prestress is simulated by using interferences at pole locations and an insertion of shims at the horizontal midplane. For each single layer the values of the shim

and interference are the same. In the third case with Al collars the (required) pole azimuthal coil stresses are lower than before and the values are 35 and 30 MPa respectively for the inner and the outer layer.

Assembling

For all cases, welding is simulated with the outer cylinder azimuthally stressed with a tension of 207 MPa. For the first geometry, this adds approximately 13 MPa with round collars and 7 MPa with anti-oval ones to both the inner and outer coils. For the second geometry the increase is also around the values mentioned above. For the third case the welding noticeably increases the pole stresses by about 75%. The values are 62 MPa for the inner and 53 MPa for the outer coil. This can be explained bearing in mind its different mechanical structure. In fact in the first two solutions, before welding there should not almost be gap between the two yoke halves and no gap after welding, while in the third, there is an average gap (it is tapered) of about 0.28 mm after welding.

Cool-down at 4.2 K

Due to the fact that two yoke halves are closed at room temperature, the pole stress in the coils for the first two geometries decreases by about 18 MPa. For the third, where the outer cylinder drives the two yoke halves to be in contact between 120 and 100 K, the drop is almost negligible for the inner and 6 MPa for the outer layer. Also, the mating force on the half-yokes in the vertical plane is 850 N. The azimuthal stress in the outer cylinder does not change for the third geometry but reaches almost 450 MPa for the others.

Energization at B= 6.8 T:

The value of the outward magnetic force is about 1000 N/mm. For the first geometry the calculations show that more than 75% of this force is taken by the collars. Due to vertically split yoke and contact at the horizontal midplane at 4.2 K between the yoke and the collars in the second geometry, almost 60% is taken by the collars and the rest is transmitted to the yoke. Due to the lower rigidity of the Aluminum collars in the third geometry the value decreases to approximately 37%. At full excitation since all the gaps in the iron yoke remain closed and therefore, as foreseen, there is practically no change in the azimuthal stress for the outer cylinder. At full excitation the coils are still in a compressive state and the pole stresses for all the cases are almost the same with an average value of about 35 MPa for the inner and outer layer. The maximum compressive stress in the coils is about 90 MPa.

Plots of the changes in the average azimuthal inner and outer coil pole stress over the course of the above mentioned loading conditions can be seen in figures 4 and 5 for the horizontally split and aluminum bar yoke configurations respectively.

Magnet and coil ends

The SSC Cold Mass magnet ends consist of several components which include the end spacers, collet end clamps, end plates and end yokes (see Figure 6). With the exception of the end yokes, these components mechanically support and rigidly restrain the superconducting coils in the magnet. The end yoke supports the skin where the iron yoke laminations end (see Figure 6) and also provides some fringe field reduction.

Coil Winding

High internal stresses in the conductor during winding occur from bends "the hard way" (7). These high stresses can create turn to turn shorts caused by insulation damage and degradation of the strands where the superconducting filaments break. High internal stresses also affect the coil to coil consistency in conductor placement. The selection of an appropriate end geometry can minimize these problems. The grouped method of stacking cables is used to minimize the stress and strain in the coil ends. An infinitely thin "guiding strip" which is numerically derived using program BEND (8) is placed inside the current block. The optimal location

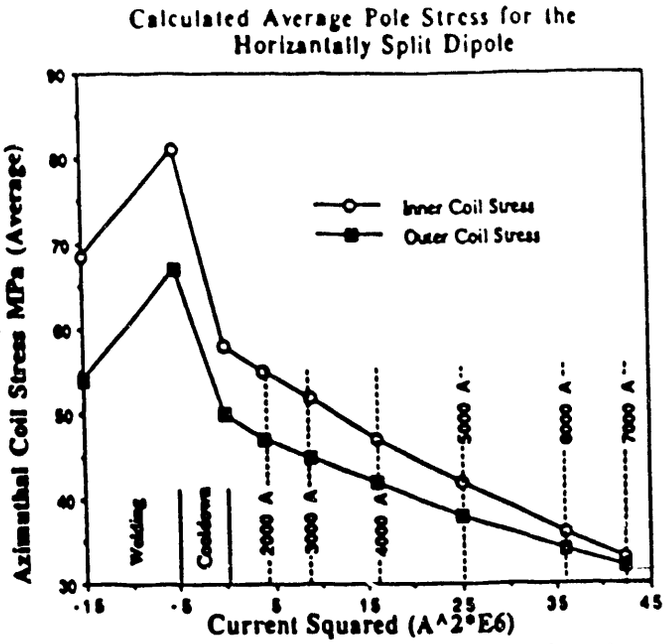

Figure 4. Calculated Average Azimuthal Pole Stress under various Loading Conditions for the Horizontally Split Dipole

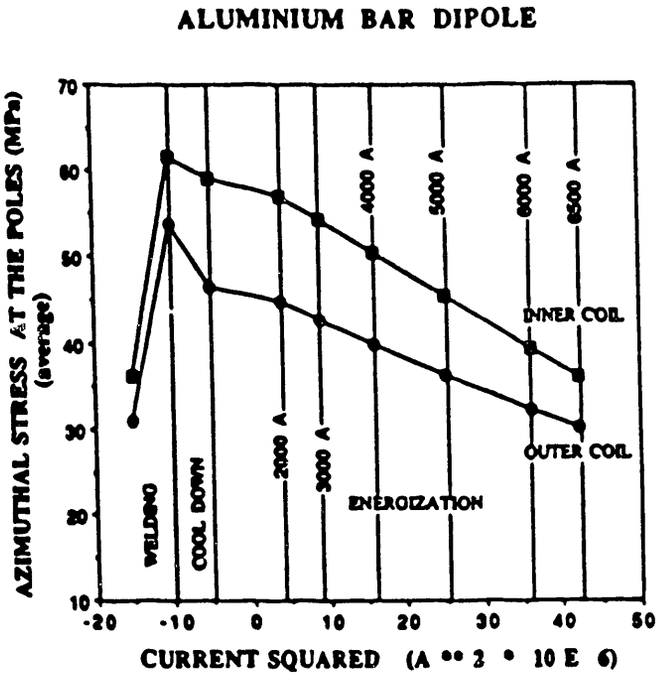

Figure 5. Calculated Average Azimuthal Pole Stress under various Loading Conditions for the Aluminium Bar Dipole

of the guiding strip is determined by minimizing strain energy and twist of the conductors. End effects have been studied to determine the exact magnetic length of a dipole as well as to improve field quality in the ends. By shifting the points at which each coil begins its bend the integrated harmonics can be minimized. This is done in two stages; first the fields for each coil are calculated analytically and the harmonics minimized without iron. Then a TOSCA® (2) model is produced of the coils together with iron, using an auxiliary program which converts the output from BEND into a number of 20 noded brick elements. The effective length and the integrated harmonics is calculated. If necessary the coil offsets can be re-iterated. Once the end geometry has been analytically optimized, surface shapes are produced from computer programs developed at Fermilab (9). All end parts including keys, saddles, fillers and spacers are made from G-10.

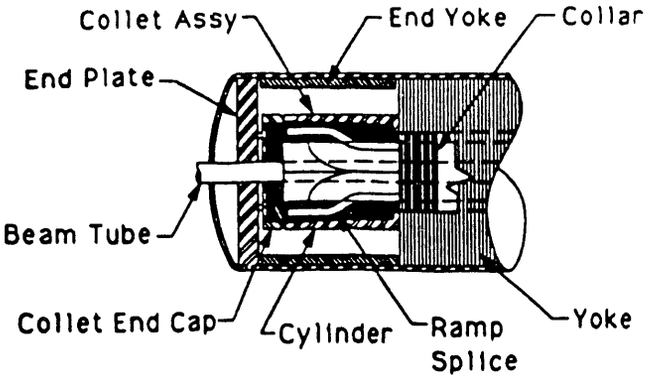

Figure 6. Cold Mass, Lead End

Collet End Clamp Design

The collet end clamp assembly is a radial clamping scheme used to support and rigidly restrain the magnet ends. The outer steel clamp has an internal conical shape. The inner material is G-10 and is made of a four quadrant construction with a matching external conical shape. The lead end assembly is identical to the return end except it includes hollowed out areas at the vertical parting plane to accept the inner to outer splices. Clamping is accomplished by applying a force to the steel clamp and G-10 parts. The assembly is completed by welding the end cap to the clamp.

End Plate

The end plate is a 38 mm thick stainless steel plate used to apply a compressive load to the collared coil assembly. The end plate supports the axial force developed during the excitation and improves quench performance.

Mechanical Design of magnet end

Low cycle fatigue stress limits must be observed for a magnet shell (skin) design to realize long term operational reliability. Critical bending stresses under pre-load and thermal load are found in the end skins of the dipole magnet. These stresses can be minimized by utilizing an end yoke extending from the body yoke to the end plate.

The proposed end shell design (10) aims at enhancing the magnet reliability and safety by minimizing the local bending stresses at the skin where the collet coil end assembly begins and the iron yoke laminations stop. The analytical results and propositions aim to optimize the design so as to limit skin stresses within the low cycle fatigue limit, specifically in the seam weld zone. The finite element code ANSYS® was used to analyze the shell under thermal, structural and magnetic loads. The skin was modeled with shell elements and the end yoke was modeled with two layers of solid element with six degrees of freedom in each node to ensure displacement compatibility with the skin. Mechanical pre-stress on the skin was input with a radial pressure of 7 MPa. Thermal loads are input with an initial temperature at 300 K and cooldown to 4K. The body yoke was modeled with areas cut-out to represent the helium tube and bus cavity to account for local stiffness effects on skin stress. The salient results of the analysis are tabulated in Table 3.

(1) The best result can be achieved by welding the end skin to a Kawasaki steel end yoke. This design will reduce the peak end shell stress by 50%, compared to the design of the end skin without an end yoke. The radial width (thickness) of the end yoke would be about 19 mm.

(2) The results of non-linear analyses with a Kawasaki steel end yoke lap-jointed to the end skin indicates that the critical end skin stress is increased by 40% in comparison to the design of end skin with a spot welded end yoke.

(3) Considering 316 LN stainless steel as the dipole magnet skin material, stresses in design A, (the end skin with welded end yoke), are 46% of the allowable stress which is the yield stress at 4 K and 1000 cycles. With design B, (lap-jointed end skin to end yoke), the end skin stresses are 66 % of the allowable stress.

END SKIN STRESS	MPa
(1) END SKIN WITH WELDED END YOKE	414
(2) END SKIN WITH LAPPED END YOKE	600
(3) END SKIN WITHOUT END YOKE	855
(4) 316 LN LOW CYCLE FATIGUE LIMIT	910
(5) CASE 3 WITH BODY YOKE @ 78 K	1165

Table 3. End Skin Stress for Various Configurations

The following conclusions are drawn:

(a) A substantial increment of stresses in the end skin if the end yoke is not welded to the skin.

(b) The magnitude of friction coefficient has negligible effect on the skin stress.

(c) The margins of safety are 1.17 and 0.51 for design (A) and (B) respectively.

Acknowledgments

This work was carried out under the auspices of the head of the Magnet Division Tom Bush and his deputy Roger Coombes who also stimulated the interlaboratory collaboration.

References

1. R.C. Gupta, S.A. Kahn and G.H. Morgan, "DSX201 - Coil and Iron Design for the SSC 50 mm Magnet with Wider Cables", to be published.

2. PE2D® and TOSCA®, Trademarks from Vector Fields Limited, Oxford, England.

3. J.R. Turner, "Mechanical Analysis of the W6733H Cross-Section", MD-TA-143, July 1990.

4. J. Kerby, "50 mm Vertical Split FE Conclusions", Presented to the 5 cm Task Force, May 23, 1990.

5. G. Spigo, " Preliminary Assessment of the Mechanical Strength of a Dipole with Aluminium Collars, Vertically Split Yoke and Curved Aluminium Bars to Control the Gap from Room to Working Temperature", MD-TA-158, June 1990.

6. ANSYS®, Trademark from SWANSON Analysis Inc., Houston, PA, U.S.A.

7. R. C. Bossert, J. M. Cook and J. S. Brandt, "End Designs for Superconducting Magnets", presented at Breckenridge Workshop, August 14-24, 1989.

8. J. M. Cook, "An Application of Differential Geometry to SSC Magnet End Winding", SSCL-N-720, April 1990.

9. R. C. Bossert, J. S. Brandt, J. A. Carson, H. J. Fulton and G. C. Lee, "Analytical Solutions to SSC Coil End", FERMILAB-Conf-89/54, March 1989.

10. K. K. Leung, "Nonlinear Stress Analysis of Superconducting Dipole Magnet Shell ", MD-TA-167, September 1990.

Disclaimer Notice

This report was prepared as an account of work sponsored by an agency of the United States Government. Neither the United States Government or any agency thereof, nor any of their employees, makes any warranty, express or implied, or assumes any legal liability or responsibility for the accuracy, completeness, or usefulness of any information, apparatus, product, or process disclosed, or represents that its use would not infringe privately owned rights. Reference herein to any specific commercial product, process, or service by trade name, trademark, manufacturer, or otherwise, does not necessarily constitute or imply its endorsement, recommendation, or favoring by the United States Government or any agency thereof. The views and opinions of authors expressed herein do not necessarily state or reflect those of the United States Government or any agency thereof.

Superconducting Super Collider Laboratory is an equal opportunity employer.

END

DATE FILMED

11/14/91